Diffraction and absorption enhancement from textured back reflectors of thin film solar cells

F.-J. Haug, A. Naqavi, C. Ballif

Ecole Polytechnique Fédérale de Lausanne (EPFL), Institute of Microengineering (IMT), Photovoltaics and Thin Film Electronics Laboratory, Rue A.-L. Breguet 2, CH-2000 Neuchâtel, Switzerland

Abstract

We study light scattering and absorption in thin film solar cells, using a model system of a sinusoidally textured silver reflector and dielectric layers of ZnO and amorphous silicon. Experimental results are compared to a theoretical model based on a Rayleigh expansion. Taking into account the explicit interface profile, the expansion converges fast and can be truncated typically after three or four orders. At the same time, the use of realistic permittivity data correctly reproduces the intensity of diffracted orders as well as the coupling to guided modes and surface plasmon polariton resonances at the silver surface. The coupling phenomena behind the light trapping process can therefore be assessed in a simple, yet accurate manner.

Introduction

In solar cells based on thin film silicon, limitations due to poor charge transport require the use of thin absorber layers [1]. Adding weak absorption because of indirect band gaps in amorphous or microcrystalline material, the feasible device thicknesses are typically below the optical absorption length; consequently, they require an optical design where the absorption is enhanced by light scattering. The most successful realizations rely on random textures [2], but at the same time it was suggested that cleverly designed periodic interface textures should be able to outperform their random counterparts [3]. Alas, it took more than a decade before suitable periodic structures for solar cell fabrication were demonstrated [4, 5], and still some time elapsed before acceptable device efficiencies were demonstrated for thin film silicon solar cells with periodic interface textures [6-13]. From a modelling point of view, periodic structures pose fewer difficulties than random ones, consequently, many reports on rigorous calculations appeared [14-19]. While increasing computing power made the modelling faster and more accurate over the years, the understanding of the actual mechanisms of light trapping is still limited.

Some insight into the underlying physics can be gained by a perturbation approach where the multilayer stack of the cell is approximated by an equivalent stack with flat interfaces; after determining the dispersion diagram of the modes that can be sustained in such a stack, the texture can be regarded as perturbation that couples external radiation to guided modes [20]. Periodic textures make the coupling mechanism particularly clear because peaks of enhanced absorption at clearly defined wavelengths can be related to resonant excitation via grating coupling [12, 21]. The understanding of the coupling process can subsequently be employed for designing more adequate grating shapes or quasi-periodic structures [22]. Ultimately, these ideas apply also to random interface texture if an adequate number of periods are superimposed. However, this approach lacks a detailed prediction of the coupling strength.

Scattering intensities from random surfaces have been widely studied for remote sensing applications using radar waves [23, 24], the calculation of diffraction intensities from grating surfaces dates back to Lord Rayleigh [25]. References [26-29] may serve as entry point to the huge body of literature on these topics. The description of gratings with covers of thin dielectric films has been developed to describe undesired tarnishing of silver or the effect of nonabsorbing protection layers for special applications [30, 31].

In this contribution, we address absorption in solar cell structures on periodic reflectors. Absorption enhancement is clearly desired for the active part of a cell, while it must be avoided in the inactive parts. For the theoretical understanding, we use a computationally simple, yet efficient diffraction theory that takes into account the shape of the interface as well as realistic permittivity data. We discuss briefly the effect of lossy dielectrics on the plane waves that serve as basis functions for the Rayleigh expansion. In the experimental part, we quantify theoretical results against measurements of diffracted light intensities from sinusoidal relief gratings covered with dielectric films. Finally, we investigate the absorption by excitation of guided modes and surface plasmon resonances.

Experimental

The experiments were carried out on a grating with sinusoidal shape with period of 890 nm and amplitude of 70 nm, resulting in a peak-to-valley depth of 140 nm. The gratings were manufactured by a commercial supplier via embossing into a UV-curable polymer (OVD Kinegram AG). We deposited three types of film on these gratings; thin films of silver and ZnO were grown at ambient temperature by DC and RF sputtering, respectively (Univex 450 B, Leybold). Silver films are 100 nm thick, the ZnO thickness varies between 0, 20, 40, and 60 nm. Films of amorphous silicon were deposited at 190°C by plasma enhanced chemical vapour deposition using a diluted gas mix of hydrogen/silane equal to two, using VHF plasma excitation at 70 MHz. The nominal film thickness is 200 nm as measured on glass reference substrates, on the metal coated substrates it is actually 260 nm.

The reflection was measured from 320 to 2000 nm in a spectrophotometer (Lambda 900, Perkin Elmer). The beam was polarized with a broad band wire grid polarizer (ProFlux PPL05C, Moxtek). The system is equipped with an integrating sphere for measurement of total and diffuse reflection with a tilt of 7°. Figure 1 illustrates the conical mounting where incident and zero order reflected beam span the horizontal plane while diffraction into positive and negative orders occurs symmetrically upwards and downwards. Using a symmetric grating profile, the intensities diffracted into negative and positive orders are identical. This configuration facilitates the interpretation of the measurements because upwards and downwards diffracted beams appear at the same wavelength and angle; the number of absorption dips is thus reduced while their signature is doubled. For the grating period of 890 nm, diffuse reflection between 445 and 890 nm consists only of the first order beams, between 297 and 445 nm it consists of first and second order beams, etc. As word of caution, we note that the detectors are located in the lower part of the integrating sphere as shown in Figure 1. Thus the downwards diffracted beams may not undergo complete randomization before hitting the detector. Even though we tried to take into account this effect in the calibration of the instrument, absolute reflection values must be interpreted with care whenever there are propagating diffraction orders, i.e. below 890 nm. We try to avoid this issue by plotting the haze which largely cancels the error introduced by the geometry of the measurement. The reflection data for longer wavelengths are much more reliable because the reflection is purely specular.

Theory

This section presents some key aspects of scattering and diffraction theory as far as needed for the experimental section. The idea is to provide a collection of formulae with consistent notation.

Scalar theory

For the geometry shown in Figure 1, we define a sinusoidal surface with period P and amplitude σ; using $g = 2\pi / P$, we can write $f(x) = \sigma \sin gx$. The intensity diffracted into p-th order is proportional to $J_p^2(4\pi\sigma/\lambda)$, the square of the Bessel function of p-th order [28]. Harvey noted that this relation applies well to s-polarization (TE) after adding a normalization which distributes the light intensity between propagating diffraction orders [32]. For s-polarization, perpendicular incidence and diffraction into first order, the haze i.e. the ratio between diffuse and total reflection $H_R = R_{\text{diff}} / R_{\text{tot}}$ is thus given by:

$$H_R^s = \frac{2 \cdot J_1^2(4\pi\sigma/\lambda)}{J_0^2(4\pi\sigma/\lambda) + 2 \cdot J_1^2(4\pi\sigma/\lambda)} \qquad \textbf{(1)}$$

The argument of the Bessel functions can be split into a wavevector $k_0 = 2\pi/\lambda$ and a term of 2σ. Harvey noted that this is essentially a paraxial approximation where the incoming as well the diffracted wave probe the full depth of the grating; the approximation can be avoided by replacing 2σ by the effective depth $2\sigma_{\text{eff}} = \sigma(\cos\theta_1 + \cos\theta_2)$ [33]. For perpendicular incidence, $\theta_1 = 0$ and $\theta_2 = \arcsin(\lambda / P)$.

An expression for the haze in p-polarization (TM) is not readily available but an indicative result for short wavelength may still be obtained by following a perturbation treatment of Maystre [34]. For perpendicular incidence, the amplitudes of first order diffraction for TE and TM polarization (eqns. (28) and (29) in ref. [34]) differ only by a factor of $\sqrt{1-(\lambda/P)^2}$. We can thus write the following:

$$H_R^p \approx \frac{\frac{2}{1-(\lambda/p)^2} \cdot J_1^2(4\pi\sigma/\lambda)}{J_0^2(4\pi\sigma/\lambda) + \frac{2}{1-(\lambda/p)^2} \cdot J_1^2(4\pi\sigma/\lambda)} \qquad \textbf{(2)}$$

Rayleigh expansion

We describe systems with one and two sinusoidal interfaces, i.e. the interface between two media or the case of a thin film with thickness d that is embedded between two semi-infinite media. Figure 1 shows the chosen coordinate system where the xy plane is spanned by the incident, reflected, and transmitted beams; the mean of level of the interfaces is oriented along the yz plane. The interfaces are assumed to be corrugated with sinusoidal shape of the same period; they are described by $f_1(x) = \sigma_1 \cdot \sin gx$ and $f_2(x) = d + \sigma_2 \cdot \sin gx$. For our experimental situation, the interfaces may vary in amplitude in the form of flattening or pinching. Because the geometry is invariant with respect to the y-coordinate, we can describe s- (or TE) and p-polarization (or TM) by directing either the electric or the magnetic field along the y-direction, reducing thus from a vectorial to an essentially scalar problem [35].

The electromagnetic field in the two half spaces as well as within the films is subsequently expanded into plane waves. Further considerations are facilitated by the Rayleigh hypothesis, i.e. assuming that the expansion remains valid in the roughness zones and at the interfaces. For sinusoidal textures, Petit showed that this assumption is valid up to $\sigma / P = 0.07$ [36], van den Berg obtained similar limits for triangular and rectangular gratings [37]. In an experimental situation similar to ours, Zaidi found reliable results up to and even beyond $\sigma / P > 0.3$ [38]. Defining the wavevector modulus in vacuum by $k_0 = 2\pi / \lambda_0$, the in-plane component of the wave vector of a wave with oblique incidence under an angle θ is given by $k_I = \sqrt{\varepsilon_I} \cdot k_0 \sin\theta$. For the experimental situation shown in Figure 1, the angle θ is defined with respect to the horizontal plane; for our conical mount it is thus equal to zero. The x-component, often called propagation constant, is given by $S_I = \sqrt{\varepsilon_I k_0^2 - k_I^2} = \sqrt{\varepsilon_I} \cdot k_0 \cos\theta$.

The reflected field is expressed as plane wave expansion with the reflection coefficients r_n. Using the reciprocal lattice vector g, their z-components are given by

$k_{I,n} = k_I + n \cdot g$, while the x-components are defined by $S_{I,n} = \sqrt{\varepsilon_I k_0^2 - k_{I,n}^2}$; n runs through negative and positive integers including zero ($n = 0, \pm 1, \pm 2, ...$). For s- and p-polarization, the respective y-components of electric and magnetic field are given by:

$$F_I = \exp\{i(S_I x + k_I z)\} + \sum_n r_n \cdot \exp\{i(-S_{I,n} x + k_{I,n} z)\} \qquad \textbf{(3)}$$

In the film, we can write $k_{II,n} = k_{I,n}$ because the in-plane components do not change upon the transition from one medium into another. The propagation constants are given by $S_{II,n} = \sqrt{\varepsilon_{II} k_0^2 - k_{II,n}^2}$ where ε_{II} denotes the relative permittivity of the film. The field is composed of forward-going waves that are diffracted from the left interface (positive along x), and waves that are diffracted backwards from the right interface (negative along x):

$$F_{II} = \sum_n a_n \cdot \exp\{i(S_{II,n} x + k_{II,n} z)\} + b_n \cdot \exp\{i(-S_{II,n} x + k_{II,n} z)\} \qquad \textbf{(4)}$$

The field in the right half space is given by transmitted waves in forward direction:

$$F_{III} = \sum_n t_n \cdot \exp\{i(S_{III,n} x + k_{III,n} z)\} \qquad \textbf{(5)}$$

Figure 2 illustrates the different wavevector components for three different materials and a wavelength of 633 nm. We use the z-component of the wavevector as principal variable because it does not change upon transition between the media. The lowest panel illustrates the situation for air; for the angular range of incident light, the in-plane component of the wave vector $k_{air} = \sqrt{\varepsilon_{air}} \cdot k_0 \sin\theta$ can vary between zero (perpendicular incidence) and $k_0 = \pm 2\pi / 633\ \text{nm} \approx \pm 9.92 \times 10^4\ \text{cm}^{-1}$ (grazing incidence under $\pm 90°$). The corresponding values of S_{air} are purely real, and according to their definition they can assume values located on the semi-circle above $\pm k_0$. According to the definitions preceding eq. (3), the expansion of the reflected field contains in-plane components of the wave vector which are larger than k_0. The corresponding propagation constants S_{air} are

thus purely imaginary. Such waves are called evanescent because they cannot propagate. The inset illustrates that the transition between real and imaginary propagation constants is sharp.

Grating coupling can be read from the same diagram, as illustrated by the vertical lines that represent the reciprocal lattice vectors of the 1D geometry with period of 890 nm. For air, the semicircle intersects with three lines, representing three propagating orders, i.e. zero and ± 1. Higher orders intersect with the evanescent branches and cannot propagate. The middle panel illustrates a slightly lossy medium with refractive index higher than air, resulting in a semi-circle with larger radius that allows propagating orders up to ± 2. The inset shows that the edges towards grazing propagation are blurred because the propagation constants are complex. Different from evanescent modes in a lossless medium, these modes can propagate by means of the finite real part but their amplitude decays rapidly by means of their imaginary part. Likewise, propagating diffraction orders inside the semi-circle keep a small imaginary part which accounts for lossy propagation. For silver, the situation is different because the propagation constants are no longer located on a semi-circle but on wide a semi-elliptical characteristic. This makes the grating couple to a wide range of modes whose large imaginary components makes them very strongly attenuated.

Boundary conditions require that the fields are continuous at both interfaces. Moreover, the normal derivative of the electric field is continuous for s-polarization; for example, the first interface requires that $\partial F_{II} / \partial n = \partial F_I / \partial n$ along the surface defined by $x = \sigma_1 \sin gz$. For p-polarization the derivative of the magnetic field is discontinuous as $(1/\varepsilon_{II}) \cdot \partial F_{II} / \partial n = (1/\varepsilon_I) \cdot \partial F_I / \partial n$. Because our geometry is invariant with respect to the y-coordinate, the normal derivative is expressed as:

$$\frac{\partial}{\partial n} = \left(1 + \left(\frac{\partial f}{\partial z}\right)^2\right)^{-1/2} \left(\frac{\partial}{\partial x} - \frac{\partial f}{\partial z}\frac{\partial}{\partial z}\right) \qquad \textbf{(6)}$$

An infinite set of equations is obtained by sorting for the orders $\exp(i \cdot n \cdot gz)$ of the plane wave expansion and the different coefficients are coupled by the derivative of the sinusoidal surface profile $\partial f_p / \partial z = (g\sigma_p / 2) \cdot (\exp(igz) + \exp(-igz))$. Difficulties with the truncation are elegantly circumvented by an additional expansion of terms that contain the sinusoidal surface profile in the exponent into Bessel functions [38-40]. For a treatment of more general surface profiles, see refs. [41, 42].

Results and discussion

We apply the concepts of the theory section to experimental results measured on relatively simple structures consisting of two or three media, e.g an opaque silver film with sinusoidal corrugation and configurations with a dielectric film on such a silver reflector.

Reflection from a corrugated surface

In this section, we regard corrugated surfaces of opaque thin films in contact to air, i.e. two media delimited by one interface; for the case of silver, even thin films of about 100 nm justify treatment as bulk material [43]. The right part of Figure 3 shows that within experimental uncertainties little or no scattering takes place for wavelengths that are larger than the grating period. Immediately after onset, the scattering intensity is much more pronounced for p- than for s-polarization. Towards wavelengths of around 500 nm, the differences become less pronounced, but p-polarization shows a distinct dip at 490 nm due to the excitation of a surface plasmon polariton resonance. The dip in the haze ratio in Figure 3 suggests that close to 60% of the reflected light gets emitted back into the specular beam at the wavelength of the resonance. Inspection of the absolute reflection data at the position of the dip (data not shown) reveals that about 25% of the incoming radiation is dissipated by the resonance.

Figure 3 includes the characteristics of scalar scattering theory according to eq. (1); the paraxial result for s-polarization overestimates the scattered intensity, but the non-

paraxial correction yields good agreement with the experimental result, corroborating the finding of Harvey [32]. The approximation for the haze in p-polarization according to eq. (2) reproduces correctly that the diffracted intensity is higher, but for wavelengths approaching the grating period, the approximation diverges quickly; the non-paraxial correction yields a slight improvement. Overall, we can conclude that the applicability of scalar theory to diffraction phenomena in reflection is capable of explaining the general trends, but its precision is limited. However, the paraxial result without any corrections is a rather acceptable approximation for unpolarized light, i.e. the average over s- and p-polarization. Because polarization effects are averaged in case of randomly textured surfaces, this would explain why in some cases scattering from natural surfaces is described successfully with the paraxial theory [44-46]. However, such an approximation cannot be assumed to apply in general.

We turn to results of the Rayleigh expansions. Dotted, dashed, and full lines in Figure 4 show the calculated haze for expansion into first, second, and third order, respectively, using tabulated data for bulk silver [47]. The first order expansion reproduces the haze curve already very well, particularly for s- polarization. In case of p-polarization, the onset at long wavelengths is overestimated, but much better than the scalar results shown in Figure 3. Expansion to second order reproduces the dip close to 490 nm and also results in a slight improvement for the onset at long wavelengths. Third order expansion yields only a marginal improvement on the depth of the dip; expansion to forth and higher orders are not distinguishable from third order.

Figure 5 shows the haze in reflection from a 260 nm thick film; the single interface model applies only in the strongly absorbing region where absorption in the film suppresses the influence of light that is reflected from the rear interface. In the shown case, this happens below 550 nm. Interestingly, the dip for p-polarization at short wavelengths is less pronounced and it occurs at a wavelength of 450 nm. This is half the grating period and represents the onset of second order diffraction. For reflection from a metallic grating, the dip was shifted to 490 nm, the resonance wavelength of the surface plasmon resonance.

The behaviour in the weakly absorbing region above 550 nm will be described at the end of the next section.

Diffraction and interference phenomena in thin films

Figure 6 shows the measured haze of a series of ZnO coatings with different thickness on the textured silver reflector. The p-polarized results in the lower panel show that the dip related to plasmon excitation moves systematically towards longer wavelengths with increasing thickness of the coating. The results for s-polarization in the upper panel show a similar dip, but only for ZnO thickness of 40 and 60 nm, and at much shorter wavelength. Different from the excitation of the surface plasmon resonance which occurs only for p-polarization, these dips are related to coupling with guided modes in the ZnO films.

For modelling, we match the boundary conditions at two interfaces. The theoretical results in Figure 6 are based on a third order expansion, using in-house data for the permittivity data of ZnO, and assuming fully conformal interfaces ($\sigma_1 = \sigma_2$). The haze characteristics match for both polarization directions and also the shift of the dip with the ZnO thickness is reproduced. The wavelengths of the dips are slightly underestimated while the predictions fall below lower than the measured values. At the same time, the widths of the dips and their tails towards lower wavelengths appear to be correct. Based on the observation that the position of the dip is underestimated also for the pure silver surface, we conclude the deviation is not related to an error in the calibration of the ZnO thickness. It appears more likely that the bulk dielectric data of silver is not applicable to our sputtered films; we will come back to this point in the next example.

The haze of the 260 nm thick silicon film on silver was already presented in Figure 5; the polarization dependence of the total reflection from this sample is shown in Figure 7. The figure includes the reflection data of a flat reference sample which shows Fabry-Perot interferences at 1300, 800, 650, and 550 nm. At shorter wavelengths the absorption is sufficiently strong to suppress interference with light reflected at the back interface; the

reflection in the visible is around 40% and gradually increases to about 55% at the lower end of the wavelength scale. On the textured samples, several absorption signatures due to the excitation of waveguide modes are overlaid. Between these resonances the total reflection is close to the flat sample, except for the p-polarized sample at short wavelengths where the texture yields an antireflection effect.

We modelled the textured silicon film again with a third order expansion, using in-house data for amorphous silicon. The dotted lines in Figure 7 represent modelled results with the data of bulk silver [47], showing that the reflection is overestimated for both, the flat as well the textured samples. We tried to describe silver with “bad” material quality with data of ion bombarded films reported by Parmigiani [48]; dashed and full lines represent their 20 eV and 40 eV samples, respectively. The flat sample appears to behave between the latter two cases. In case of the textured samples, even the 40 eV data underestimates the absorption for most of the guided modes. Exceptions are found at 1150 nm in s-polarization and for p-polarization at 1050 and 1250 nm where the absorption is massively overestimated even when the data of bulk silver is used. The width of resonances is met for none of the signatures beyond 800 nm. Below that wavelength the correspondence is better and at first glance there is only little sensitivity to the properties of silver. We can tentatively conclude that the absorption phenomena are dominated by silicon. However, we note that even if the influence of silver appears to be a secondary effect, it is still noticeable in applications [49].

Figure 8 plots again the haze of the 260 nm a-Si thick film from Figure 5. Overlaid are modelled results, this time taking into account both interfaces rather than bulk material. Compared to Figure 5, the main features at 600 nm and between 700 and 800 nm are reproduced. For both polarizations, peaks and dips are overestimated, for p-polarization the combination of dip and peak at 600 nm is even inversed. Nevertheless, the overall agreement is reasonable. Finally, we note that a small improvement on the peak positions can be obtained by imposing a slightly higher amplitude to the front surface. The difference between dashed and full lines corresponds to replacing a conformal interface

with amplitude of 70 nm by one where the back is kept at 70 while the front is increased to 72 nm. The increased amplitude at the front of the structure appears surprising as the growth of thin films usually flattens underlying textures. However, growth of silicon by PE-CVD can pinch over valleys or depressions. It would be necessary to determine the actual shape of our sample by a cross-sectional analysis.

Conclusions

We presented an experimental and theoretical study of reflection and light scattering from metallic reflectors and thin films with sinusoidal texture. The theoretical results are based on a plane wave expansion that takes into account the analytic interface profile and includes realistic permittivity data of the actual materials. Comparison with experimental data shows that the expansion converges rapidly, typically within three or four orders. Nevertheless, the intensity of diffracted modes and coupling to internal waveguide modes as well as to surface plasmon polariton resonances is correctly reproduced. We are therefore confident that the theory can be applied to more complicated configurations. For example, disentangling desired and undesired absorption effects in a solar cell stack requires the inclusion of the front contact and a buffer layer at the back.

Acknowledgements

This work was funded by the European Union within the project Silicon-Light (contract number 241277) and by the Swiss National Science Foundation (contract 200020_137700/1). We thankfully acknowledge discussions with Z. Holman and D. Dominé.

References

1. D. E. Carlson and C. R. Wronski, *Amorphous Si solar cell.* Applied Physics Letters, 1976. **28**(11): p. 671-673.
2. H. W. Deckman, C. R. Wronski, H. Witzke, and E. Yablonovitch, *Optically enhanced amorphous silicon solar cells.* Applied Physics Letters, 1983. **42**(11): p. 968-970.
3. P. Sheng, A. N. Bloch, and R. S. Stepleman, *Wavelength-selective absorption enhancement in thin-film solar cells.* Applied Physics Letters, 1983. **43**: p. 579.
4. C. Heine and R. H. Morf, *Submicrometer gratings for solar energy applications.* Applied Optics, 1995. **34**(14): p. 2476-2482.
5. C. Eisele, C. E. Nebel, and M. Stutzmann, *Periodic light coupler gratings in amorphous thin film solar cells.* Journal of Applied Physics, 2001. **89**: p. 7722.
6. A. V. Shah, M. Vanecek, J. Meier, F. Meillaud, J. Guillet, D. Fischer, C. Droz, X. Niquille, S. Fa, and E. Vallat-Sauvain, *Basic efficiency limits, recent experimental results and novel light-trapping schemes in a-Si: H, µc-Si: H and micromorph tandem'solar cells.* Journal of Non-Crystalline Solids, 2004. **338**: p. 639-645.
7. N. Senoussaoui, M. Krause, J. Müller, E. Bunte, T. Brammer, and H. Stiebig, *Thin-film solar cells with periodic grating coupler.* Thin Solid Films, 2004. **451**: p. 397-401.
8. F.-J. Haug, T. Söderström, M. Python, V. Terrazzoni-Daudrix, X. Niquille, and C. Ballif, *Development of micromorph tandem solar cells on flexible low cost plastic substrates.* Solar Energy Materials and Solar Cells, 2009. **93**: p. 884-8877.
9. V. E. Ferry, M. A. Verschuuren, H. Li, R. E. I. Schropp, H. A. Atwater, and A. Polman, *Improved red-response in thin film a-Si: H solar cells with soft-imprinted plasmonic back reflectors.* Applied Physics Letters, 2009. **95**: p. 183503.
10. T. Söderström, F. J. Haug, X. Niquille, V. Terrazoni-Daudrix, and C. Ballif, *Asymmetric intermediate reflector for tandem micromorph thin film silicon solar cells.* Applied Physics Letters, 2009. **94**: p. 063501.
11. J. Zhu, C. M. Hsu, Z. Yu, S. Fan, and Y. Cui, *Nanodome solar cells with efficient light management and self-cleaning.* Nano Letters, 2009. **10**(6): p. 1979-1984.
12. K. Söderström, F. Haug, J. Escarré, O. Cubero, and C. Ballif, *Photocurrent increase in n-i-p thin film silicon solar cells by guided mode excitation via grating coupler.* Applied Physics Letters, 2010. **96**: p. 213508.
13. U. Paetzold, E. Moulin, D. Michaelis, W. Böttler, C. Wächter, V. Hagemann, M. Meier, R. Carius, and U. Rau, *Plasmonic reflection grating back contacts for microcrystalline silicon solar cells.* Applied Physics Letters, 2011. **99**(18): p. 181105.

14. C. Haase and H. Stiebig, *Thin-film silicon solar cells with efficient periodic light trapping texture.* Applied Physics Letters, 2007. **91**(6): p. 061116.

15. C. Rockstuhl, F. Lederer, K. Bittkau, and R. Carius, *Light localization at randomly textured surfaces for solar-cell applications.* Applied Physics Letters, 2007. **91**: p. 171104.

16. M. Vanecek, O. Babchenko, A. Purkrt, J. Holovsky, N. Neykova, A. Poruba, Z. Remes, J. Meier, and U. Kroll, *Nanostructured three-dimensional thin film silicon solar cells with very high efficiency potential.* Applied Physics Letters, 2011. **98**: p. 163503.

17. A. Naqavi, K. Söderström, F. J. Haug, V. Paeder, T. Scharf, H. P. Herzig, and C. Ballif, *Understanding of photocurrent enhancement in real thin film solar cells: towards optimal one-dimensional gratings.* Optics Express, 2011. **19**(1): p. 128-140.

18. A. Campa, O. Isabella, R. van Erven, P. Peeters, H. Borg, K. J., T. M., and M. Zeman, *Optimal design of periodic surface texture for thin film a-Si: H solar cells.* Progress in Photovoltaics: Research and Applications, 2010. **18**(3): p. 160-167.

19. C. M. Hsu, C. Battaglia, C. Pahud, Z. Ruan, F. J. Haug, S. Fan, C. Ballif, and Y. Cui, *High-efficiency amorphosu silicon solar cell on a periodic nanocone back reflector.* Advanced Energy Materials, 2012.

20. F.-J. Haug, T. Söderström, O. Cubero, V. Terrazoni-Daudrix, and C. Ballif, *Influence of the ZnO buffer on the guided mode structure in Si/ZnO/Ag multilayers* Journal of Applied Physics, 2009. **106**: p. 044502.

21. V. E. Ferry, M. A. Verschuuren, H. B. T. Li, E. Verhagen, R. J. Walters, R. E. I. Schropp, H. A. Atwater, and A. Polman, *Light trapping in ultrathin plasmonic solar cells.* Optics Express, 2010. **18**(S2): p. A237-A245.

22. C. Battaglia, C. M. Hsu, K. Söderström, J. Escarré, F. J. Haug, M. Charrière, M. Boccard, M. Despeisse, D. Alexander, M. Cantoni, Y. Cui, and C. Ballif, *Light Trapping in Solar Cells: Can Periodic Beat Random?* ACS nano, 2012.

23. S. Rice, *Reflection of electromagnetic waves from slightly rough surfaces.* Communications on Pure and Applied Mathematics, 1951. **4**(2-4): p. 351-378.

24. H. Davies, *The reflection of electromagnetic waves from a rough surface.* Proceedings of the Institute of Electrical Engineers, 1954. **101**: p. 209.

25. L. Rayleigh, *On the dynamical theory of gratings.* Proceedings of the Royal Society of London. Series A, Containing Papers of a Mathematical and Physical Character, 1907. **79**(532): p. 399-416.

26. R. Petit, *Electromagnetic theory of gratings*. Topics in Current Physics. Vol. 22. 1980: Springer.

27. M. Nevière and E. Popov, *Light propagation in periodic media: differential theory and design*. Vol. 81. 2003: Marcel Dekker.

28. P. Beckmann and A. Spizzichino, *The scattering of electromagnetic waves from rough surfaces*. 1987, Norwood (MA) Artech House, Inc.

29. A. Maradudin, *Light scattering and nanoscale surface roughness*. 2007: Springer Verlag.

30. M. Hutley, J. Verrill, R. C. M. Phedran, M. Nevière, and P. Vincent, *Presentation and verification of a differential formulation for the diffraction by conducting gratings.* Nouvelle Revue d'Optique, 1975. **6**: p. 87.

31. D. Maystre, *A new general integral theory for dielectric coated gratings.* Journal of the Optical Society of America, 1978. **68**(4): p. 490-495.

32. J. Harvey, C. Vernold, A. Krywonos, and P. Thompson, *Diffracted radiance: a fundamental quantity in nonparaxial scalar diffraction theory.* Applied Optics, 1999. **38**: p. 6469-6481.

33. J. Harvey, A. Krywonos, and D. Bogunovic, *Nonparaxial scalar treatment of sinusoidal phase gratings.* Journal of the Optical Society of America A, 2006. **23**(4): p. 858-865.

34. D. Maystre, O. M. Mendez, and A. Roger, *A new electromagnetic theory for scattering from shallow rough surfaces.* Journal of Modern Optics, 1983. **30**(12): p. 1707-1723.

35. J. D. Jackson, *Classical Electrodynamics*. 3 ed. 1963: John Wiley & Sons.

36. R. Petit and M. Cadilhac, *Sur la diffraction d'une onde plane par un reseau infiniment conducteur.* Comptes Rendus le l'Academie des Sciences B, 1966. **262**: p. 468.

37. P. Van den Berg and J. Fokkema, *The Rayleigh hypothesis in the theory of reflection by a grating.* Journal of the Optical Society of America, 1979. **69**(1): p. 27-31.

38. S. H. Zaidi, M. Yousaf, and S. R. J. Brueck, *Grating coupling to surface plasma waves. I. First-order coupling.* Journal of the Optical Society of America B, 1991. **8**(4): p. 770-779.

39. V. Kiselev, *Diffraction coupling of radiation into a thin-film waveguide.* Soviet Journal of Quantum Electronics, 1975. **4**: p. 872.

40. S. D. Gupta, G. Varada, and G. Agarwal, *Surface plasmons in two-sided corrugated thin films.* Physical Review B, 1987. **36**(12): p. 6331.

41. S. H. Zaidi, M. Yousaf, and S. R. J. Brueck, *Grating coupling to surface plasma waves. II. Interactions between first-and second-order coupling.* Journal of the Optical Society of America B, 1991. **8**(6): p. 1348-1359.

42. S. H. Zaidi, D. Reicher, B. Draper, J. McNeil, and S. Brueck, *Characterization of thin Al films using grating coupling to surface plasma waves.* Journal of Applied Physics, 1992. **71**(12): p. 6039-6048.

43. F.-J. Haug, T. Söderström, O. Cubero, V. Terrazzoni-Daudrix, and C. Ballif, *Plasmonic absorption in textured silver back reflectors of thin film solar cells.* Journal of Applied Physics, 2008. **104**: p. 064509.

44. K. Jäger and M. Zeman, *A scattering model for surface-textured thin films.* Applied Physics Letters, 2009. **95**: p. 171108.

45. D. Dominé, F. J. Haug, C. Battaglia, and C. Ballif, *Modeling of light scattering from micro- and nanotextured srufaces.* Journal of Applied Physics, 2010. **107**: p. 044504-8.

46. M. Schulte, K. Bittkau, K. Jäger, M. Ermes, M. Zeman, and B. E. Pieters, *Angular resolved scattering by a nano-textured ZnO/silicon interface.* Applied Physics Letters, 2011. **99**: p. 111107.

47. P. B. Johnson and R. W. Christy, *Optical constants of the noble metals.* Physical Review B, 1972. **6**(12): p. 4370.

48. F. Parmigiani, E. Kay, T. Huang, J. Perrin, M. Jurich, and J. D. Swalen, *Optical and electrical properties of thin silver films grown under ion bombardment.* Physical Review B, 1986. **33**(2): p. 879.

49. K. Söderström, F. J. Haug, J. Escarré, C. Pahud, R. Biron, and C. Ballif, *Highly reflective nanotextured sputtered silver back reflector for flexible high efficiency n-i-p thin film silicon solar cells.* Solar Energy Materials and Solar Cells, 2011. **95**(12): p. 3585-3591.

Figure captions

Figure 1: Configuration of the measurement geometry in the integrating sphere. Incident and reflected beams span the horizontal plane, diffracted beams propagate upwards and downwards; the latter can hit the detector before being randomized.

Figure 2: Illustration of the propagation constant *S* in the different materials as function of the wavevector component parallel to the interface, using a wavelength of 633 nm. Full and dashed lines illustrate the real and imaginary part, respectively. The vertical lines represent reciprocal lattice vectors of the grating with period of 890 nm.

Figure 3: Measured reflection haze of a sinusoidally textured silver surface with period of 890 nm for perpendicular incidence with s- (squares) and p-polarized light (circles). Dashed and full lines represent results of scalar scattering theory before and after correction for the effective depth of the texture, respectively.

Figure 4: Same experimental data as Figure 3. Dotted, dashed and full lines illustrate results of the plane wave expansion to first, second, and third order, respectively.

Figure 5: Measured haze from a 260 nm thick a-Si film on the grating; squares and circles represent s- and p-polarization, respectively. The solid line shows the calculated haze for reflection from corrugated bulk a-Si.

Figure 6: Haze of the sinusoidal silver surface covered with thin films of ZnO; squares reproduce the properties of the pure silver surface from Figure 3, circles, up-, and down triangles denote film thicknesses of 20, 40, and 60 nm, respectively. The overlaid lines illustrate theoretical results for expansion to third order.

Figure 7: Total reflection of a 260 nm thick film of a-Si on the textured silver reflector; squares and circles denote p- and s-polarization, respectively. In the inset, diamonds illustrate the reflection from

a flat reference sample. In all panels, the lines show theoretical results for expansion to third order using the dielectric data of bulk silver (dots) and two models of silver with reduced material quality (dashed and full lines).

Figure 8: Haze of the 260 nm thick a-Si film on the textured silver reflector (same as Figure 5). Dashed and full lines denote theoretical results for conformal and non-conformal covering, respectively, using an expansion to third order and the data of bulk silver.

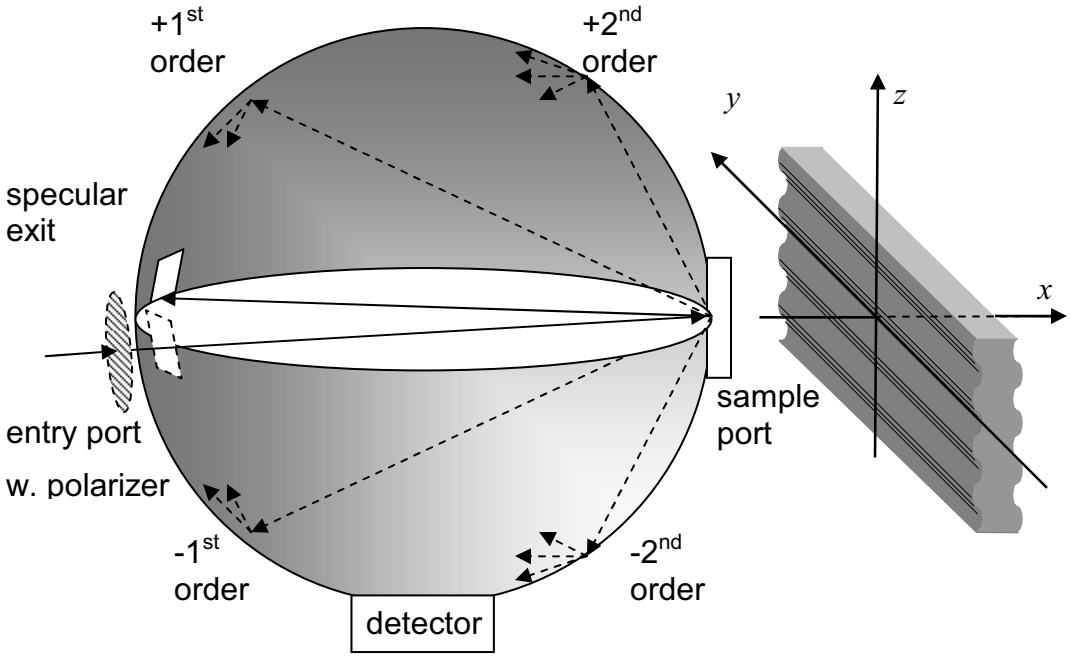

Figure 1: Configuration of the measurement geometry in the integrating sphere. Incident and reflected beams span the horizontal plane, diffracted beams propagate upwards and downwards; the latter can hit the detector before being randomized.

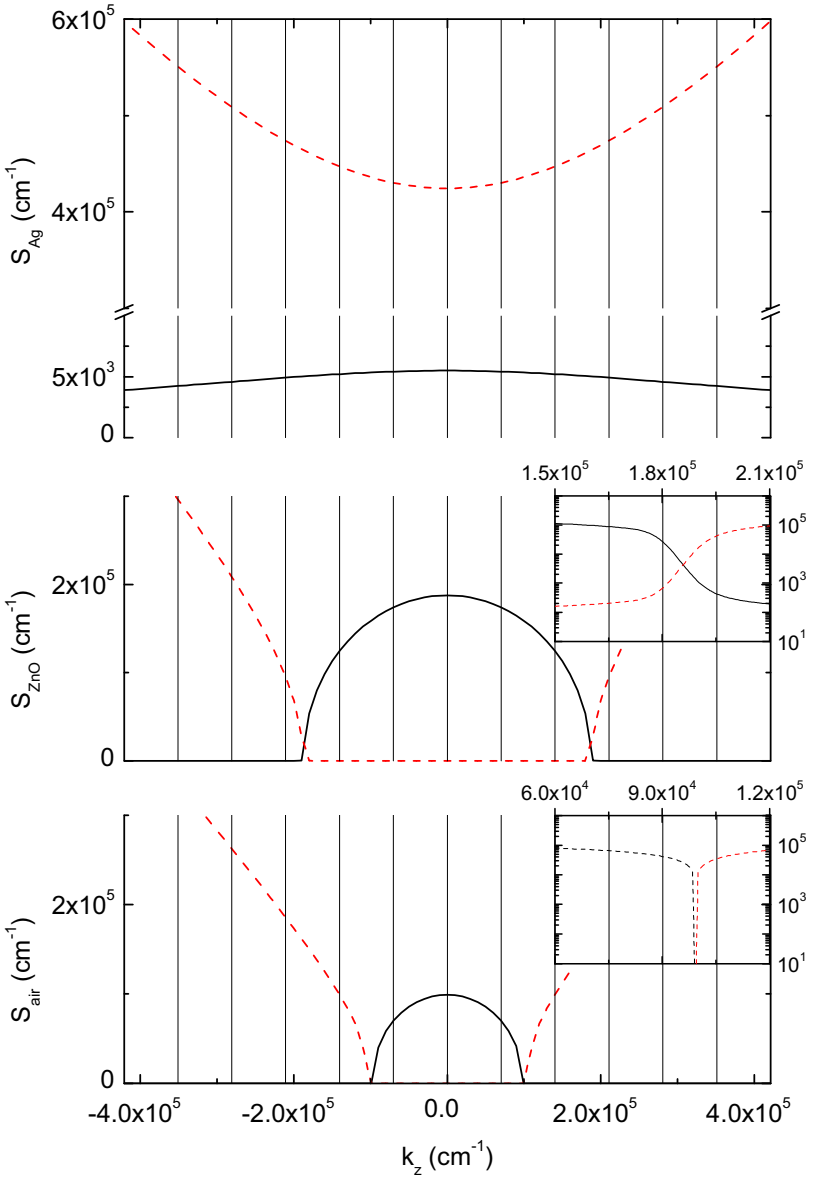

Figure 2: Illustration of the propagation constant *S* in the different materials as function of the wavevector component parallel to the interface, using a wavelength of 633 nm. Full and dashed lines illustrate the real and imaginary part, respectively. The vertical lines represent reciprocal lattice vectors of the grating with period of 890 nm.

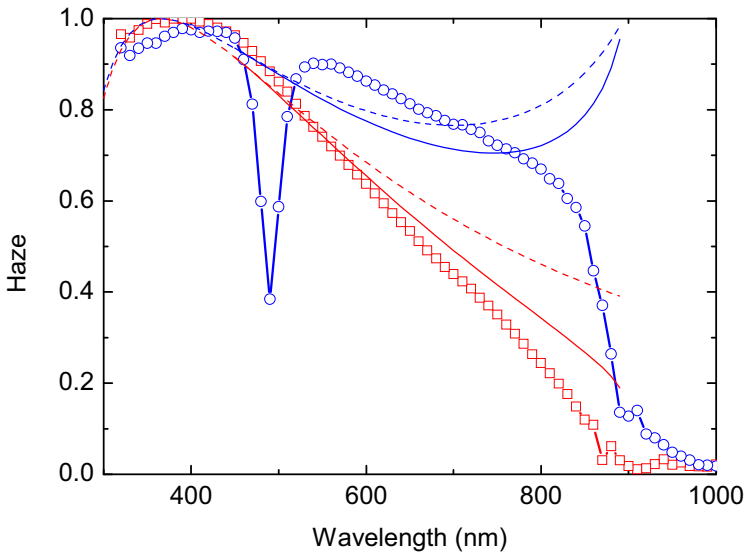

Figure 3: Measured reflection haze of a sinusoidally textured silver surface with period of 890 nm for perpendicular incidence with s- (squares) and p-polarized light (circles). Dashed and full lines represent results of scalar scattering theory before and after correction for the effective depth of the texture, respectively.

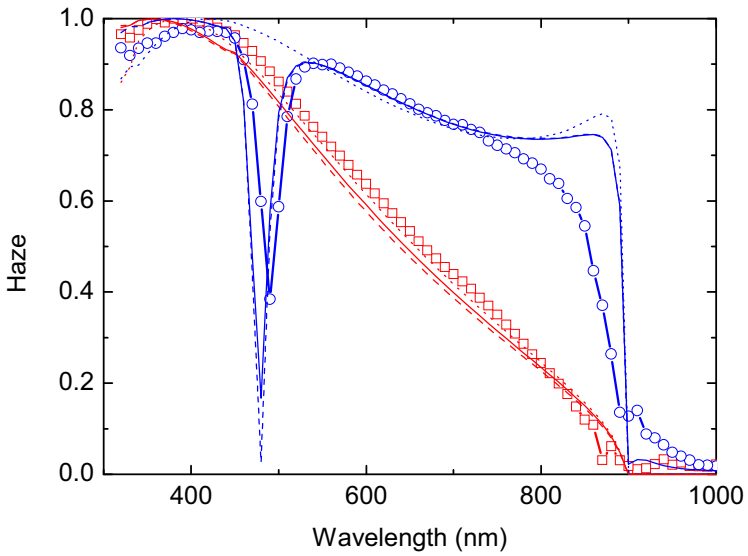

Figure 4: Same experimental data as Figure 3. Dotted, dashed and full lines illustrate results of the plane wave expansion to first, second, and third order, respectively.

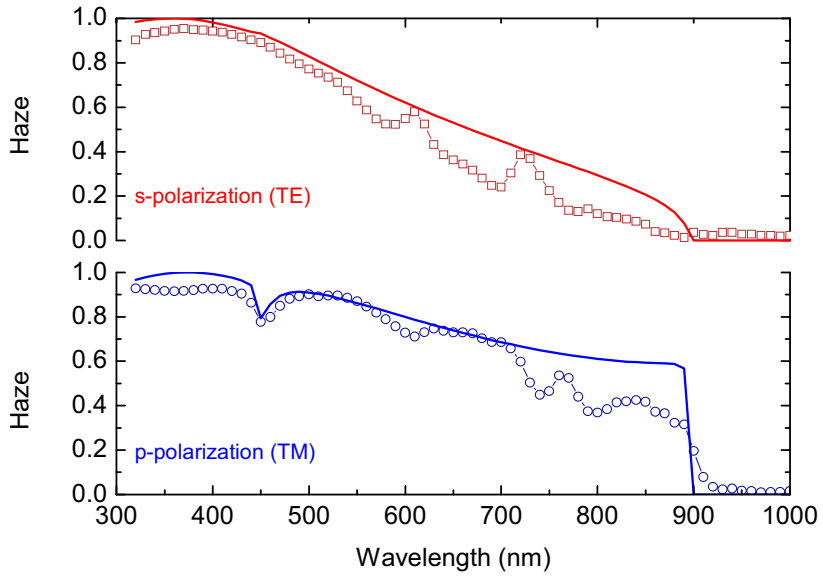

Figure 5: Measured haze from a 260 nm thick a-Si film on the grating; squares and circles represent s- and p-polarization, respectively. The solid line shows the calculated haze for reflection from corrugated bulk a-Si.

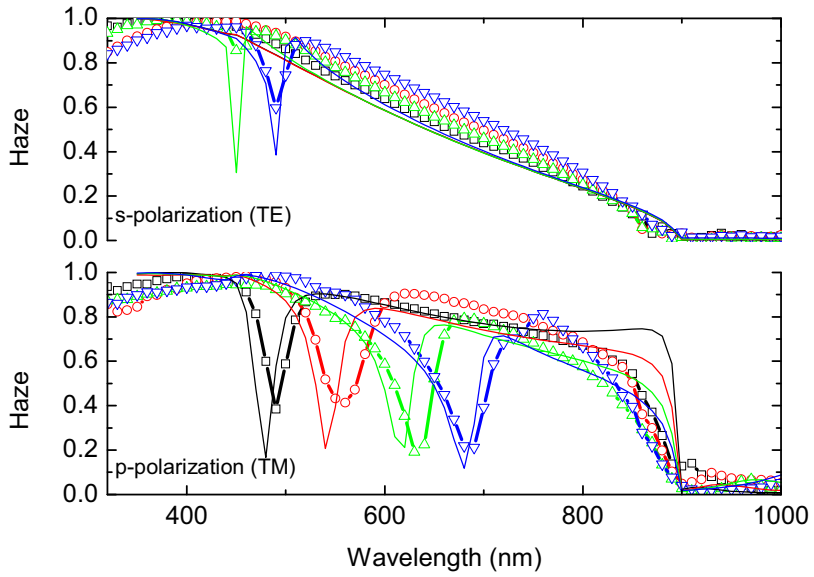

Figure 6: Haze of the sinusoidal silver surface covered with thin films of ZnO; squares reproduce the properties of the pure silver surface from Figure 3, circles, up-, and down triangles denote film thicknesses of 20, 40, and 60 nm, respectively. The overlaid lines illustrate theoretical results for expansion to third order.

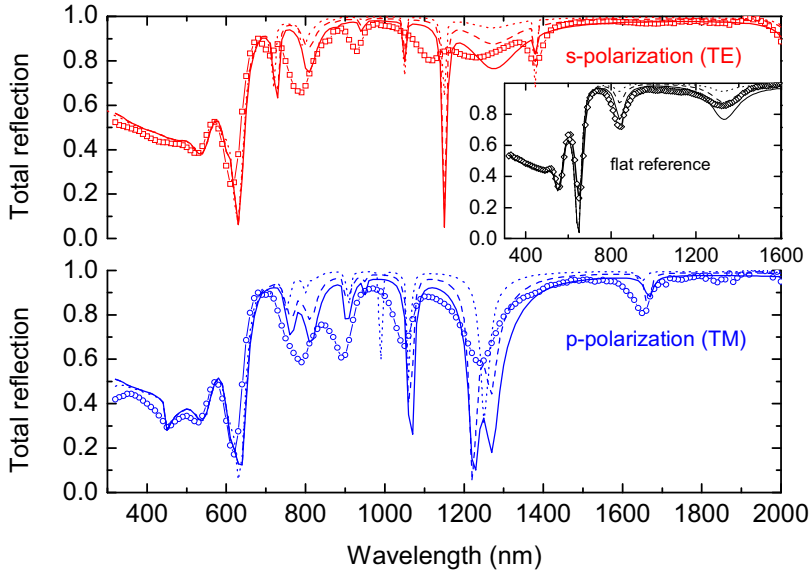

Figure 7: Total reflection of a 260 nm thick film of a-Si on the textured silver reflector; squares and circles denote p- and s-polarization, respectively. In the inset, diamonds illustrate the reflection from a flat reference sample. In all panels, the lines show theoretical results for expansion to third order using the dielectric data of bulk silver (dots) and two models of silver with reduced material quality (dashed and full lines).

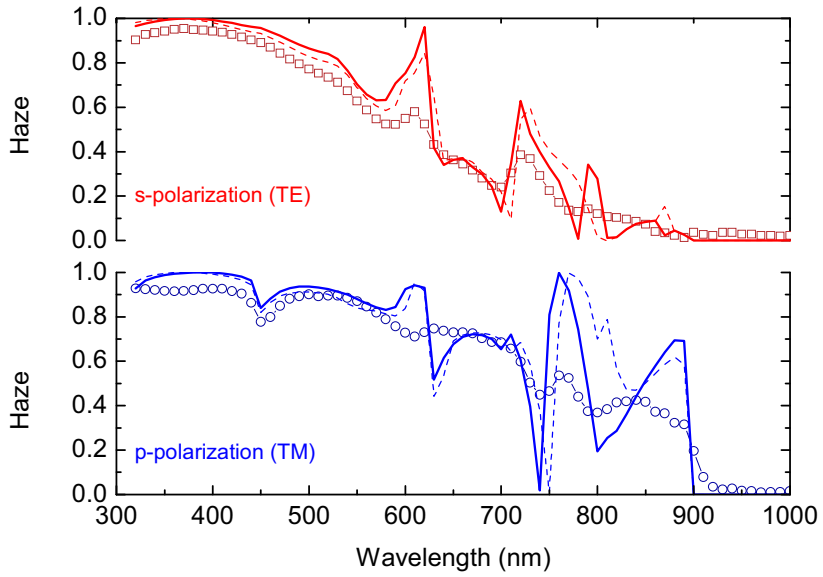

Figure 8: Haze of the 260 nm thick a-Si film on the textured silver reflector (same as Figure 5). Dashed and full lines denote theoretical results for conformal and non-conformal covering, respectively, using an expansion to third order and the data of bulk silver.